Remarkable Accelerating Effects of Ammonium Cations on Electron-Transfer Reactions of Quinones by Hydrogen Bonding with Semiquinone Radical Anions

Ken Okamoto,[†] Kei Ohkubo,[†] Karl M. Kadish,*[,‡] and Shunichi Fukuzumi*[,†]

Department of Material and Life Science, Graduate School of Engineering, Osaka University, CREST, Japan Science and Technology Agency, Suita, Osaka 565-0871, Japan, and Department of Chemistry, University of Houston, Houston, Texas 77204-5003

Received: August 31, 2004; In Final Form: September 16, 2004

Remarkable accelerating effects of the ammonium cation (NH_4^+) have been observed on photoinduced electron-transfer reactions from the triplet excited state of tetraphenylporphyin (H_2P) to quinones [*p*-benzoquinone (Q) and naphthoquinone (NQ)] in dimethyl sulfoxide (DMSO). The tetrabutylammonium cation (NBu_4^+) is also effective to accelerate the electron-transfer reduction of Q and NQ in dichloromethane (CH_2Cl_2). The hydrogen bonding interaction between the semiquinone radical anion ($Q^{\bullet-}$ or $NQ^{\bullet-}$) and NH_4^+ was confirmed by the ESR spectra of the $Q^{\bullet-}/NH_4^+$ and $Q^{\bullet-}/(NH_4^+)_2$ [$NQ^{\bullet-}/NH_4^+$ and $NQ^{\bullet-}/(NH_4^+)_2$] complexes in DMSO. Accelerating effects of NH_4^+ in DMSO and NBu_4^+ in CH_2Cl_2 on the rates of photoinduced electron-transfer reduction of Q by H_2P result from the positive shift of the E_{red} value of quinones together with a constant E_{ox} value of H_2P determined from cyclic voltammetry measurements. The driving force dependence of the rate constants for photoinduced electron-transfer reduction of quinones in the presence of various concentrations of ammonium cations was evaluated in light of the Marcus theory of electron transfer.

Introduction

The catalytic role of metal cations in enzymatic redox reactions has merited recent attention, since a growing number of redox enzymes have been demonstrated to involve metal cations at their active sites.[1−7] Since most redox coenzymes contain a lone pair of heteroatoms, an interaction of the redox cofactor with metal cations results in enhancement of the redox activity of the enzymes.[8] A number of thermal and photoinduced electron-transfer reactions have been demonstrated to be activated by interaction between metal cations and the one-electron reduced species of electron acceptors.[9−19] Not only metal cations but also organic cations such as ammonium ion have been shown to influence reactivity of the quinone cofactor in the amine-oxidation reaction and in electron transfer from the reduced quinone cofactor to amicyanin.[20−23] In such a case, hydrogen bond formation between the quinone cofactor and the ammonium ion may play an important role in controlling the electron-transfer reactions. Hydrogen bonding indeed plays a crucial role in electron transfer between two ubiquinones (Q_A and Q_B) through the iron-histidine bridge in bacterial photosynthetic reaction centers.[24−27] The positively charged iron that polarizes the imidazole ring of histidine is suggested to strengthen the hydrogen bond with Q_B, leading to a negative shift of the one-electron reduction potential of Q_B.[27] In such a case, the ammonium cation may further activate the electron-transfer reduction of quinones. The interaction between ammonium ions and reduced quinone may be further enhanced in the protein environment which is rather nonpolar with a low dielectric constant (ϵ) of ca. 2.[28] However, such effects of ammonium cations on the reactivity in the electron-transfer reduction of quinones or on the one-electron reduction potentials of quinones have yet to be clarified, because ammonium cations have generally been believed to be inert in electron-transfer reactions.[29−32] In fact, ammonium cations such as tetra-*n*-butylammonium salts are commonly employed as "inert" electrolytes in electrochemical measurements.[30−32]

We report herein the remarkable accelerating effects of ammonium cations on the rates of the photoinduced electron-transfer reactions of quinones [*p*-benzoquinone (Q) and naphthoquinone (NQ)] by hydrogen bonding or electronic interaction of ammonium cations with semiquinone radical anion in accordance with the changes of one-electron reduction potentials of quinones. The hydrogen bonding interaction between $Q^{\bullet-}$ ($NQ^{\bullet-}$) and NH_4^+ was confirmed by ESR measurements in DMSO. Determination of redox potentials with a large variation of ammonium cation concentration is made possible even in a low polarity solvent such as dichloromethane (CH_2Cl_2) by using a microelectrode in a microcell that requires only small concentrations of an electrolyte (see Experimental Section).[30,31b] The effects of NH_4PF_6 and NBu_4PF_6 on the redox potentials of quinones in several solvents are compared with what is observed for porphyrins, hexyl viologen, and $Ru(bpy)_3^{2+}$ (bpy = 2,2′-bipyridine), which exhibit little or no effect of NBu_4PF_6 on their redox potentials. The driving force dependence of the observed rate constants of photoinduced electron transfer from the triplet excited state of the porphyrins to quinones was determined in solutions having a large variation of ammonium cation concentration and evaluated in light of the Marcus theory of electron transfer.[33] The present study provides valuable insights into the important role of ammonium cations in controlling biological redox reactions.

* To whom correspondence should be addressed. E-mail: (S.F.) fukuzumi@ap.chem.eng.osaka-u.ac.jp; (K.M.K.) Kkadish@uh.edu.
† Osaka University.
‡ University of Houston.

10.1021/jp046078+ CCC: $27.50
Published on Web 11/03/2004

Experimental Section

Materials. 1,4-Benzoquinone (Q) and 1,4-naphthoquinone (NQ) were commercially obtained and purified using standard methods.[34] Tris(2,2′-bipyridyl)ruthenium dichloride hexahydrate ($Ru(bpy)_3Cl_2 \cdot 6H_2O$) was obtained commercially from Sigma-Aldrich Co., USA. 5,10,15,20-Tetraphenyl-21*H*, 23*H*-porphine (H_2P) and 5,10,15,20-tetraphenyl-21*H*, 23*H*-porphine zinc(II) (ZnP) were purchased from Aldrich. The synthesized 1,1-dihexyl-4,4′-dipyridinium dibromide and the corresponding diperchlorate salt (hexyl viologen: HV^{2+}) were described previously.[35,36] 1,4-Benzoquinone-d_4 (98at.%) was purchased from Aldrich Co. Benzonitrile (PhCN) was purchased from Aldrich Co., USA and Tokyo Kasei Organic Chemicals, Japan and purified by successive distillation over P_2O_5.[34] Dichloromethane (CH_2Cl_2), acetonitrile (MeCN), and dimethyl sulfoxide (DMSO) were received from Aldrich Co. and used as received without further purification. Tetra-*n*-butylammonium hexafluorophosphate (NBu_4PF_6), tetra-*n*-butylammonium perchlorate (NBu_4ClO_4), and tetra-*n*-butylammonium bromide (NBu_4Br) were purchased from Aldrich Co., purified using standard methods,[34] and dried under vacuum at 40 °C for at least one week prior to use. Ammonium hexafluorophosphate (NH_4PF_6) was purchased from Aldrich and used as received without further purification. Dimeric 1-benzyl-1,4-dihydronicotinamide [$(BNA)_2$] was prepared according to the literature.[37]

Electrochemical Measurements. Cyclic voltammetry (CV) measurements were performed on an EG&G model 173 potentiostat coupled with an EG&G model 175 universal programmer in deaerated solutions containing the supporting electrolyte at 298 K. A three-electrode system was used, consisting of a ~10 μm diam Pt disk microelectrode as a working electrode, a platinum wire counter electrode, and a saturated calomel reference electrode (SCE). The microelectrode is used in order to keep the ohmic drop small. In the case of very small currents, glassy carbon (3 mm diameter) was used as the working electrode. The reference electrode was separated from the bulk of the solution by a fritted-glass bridge filled with the solvent/supporting electrolyte mixture; the concentration of supporting electrolyte in the bridge was the same as that in the sample solution. In the absence of salt, however, the reference electrode contained supporting electrolyte (0.10 M). Ferricenium ion/ferrocene (Fc^+/Fc) was used as an internal standard. MeCN, PhCN, and DMSO solutions containing samples and electrolyte were deoxygenated by argon for 10 min prior to the measurements. CH_2Cl_2 solutions were deoxygenated by argon for 5 min prior to the measurements.

Time-Resolved Absorption Measurements. Nanosecond transient absorption measurements were carried out using a Panther OPO pumped by a Nd:YAG laser (Continuum, SLII-10, 4−6 ns fwhm) at 515 nm with the power of 20 mJ as an excitation source. DMSO solutions were deoxygenated by argon purging for 15 min prior to the measurements. CH_2Cl_2 solutions were deaerated by five freeze−pump−thaw cycles.

Fluorescence Quenching. Quenching experiments of the fluorescence of H_2P were carried out on a SHIMADZU spectrofluorophotometer (RF-5000). The excitation wavelength of H_2P was set at $\lambda = 425$ nm in CH_2Cl_2 or DMSO. The monitoring wavelength corresponds to the maximum of the fluorescence band at $\lambda_{max} = 652$ nm. Typically, a CH_2Cl_2 solution was deaerated by five freeze−pump−thaw cycles. A DMSO solution was deaerated by argon purging for 15 min prior to the measurements. There was no change in the spectral shape and λ_{max} due to weak binding in the steady state but there was a change in the intensity of the fluorescence spectrum by addition of a quencher and ammonium salts. The Stern−Volmer relationship (eq 1) was obtained for the ratio of the fluorescence intensities in the absence and presence of quinone

$$I_0/I = 1 + K_{SV}[Q] \quad (1)$$

derivatives. The observed quenching rate constants of photoinduced electron transfer k_{et} ($= K_{SV}\tau^{-1}$) were obtained from the Stern−Volmer constants K_{SV} and the fluorescence lifetime τ. The fluorescence lifetimes of H_2P were determined as $\tau =$ 10.8 ns in CH_2Cl_2 and 12.6 ns in DMSO by an exponential curve fit of the fluorescence decay using a microcomputer. Time-resolved fluorescence spectra were measured by a Photon Technology International GL-3300 with a Photon Technology International GL-302, nitrogen laser/pumped dye laser system (50 ps pulse duration), equipped with a four channel digital delay/pulse generator (Stanford Research System Inc. DG535) and a motor driver (Photon Technology International MD-5020). The excitation wavelength was 425 nm using POPOP (Wako Pure Chemical Ind. Ltd., Japan) as a dye in toluene. All samples were excited at 425 nm with a repetition rate of 10 Hz (pulse width 3−4 ns), and the fluorescence signal was analyzed after passing through a monochromator set at the peak emission of the corresponding sample.

ESR Measurements. The ESR spectra of ammonium ion complexes of semiquinone radical anions were recorded on a JEOL X-band spectrometer (JES−RE1XE) with a quartz ESR tube (1.2 mm i.d.). The ESR spectra were measured under nonsaturating microwave power conditions. The magnitude of modulation was chosen to optimize the resolution and the signal-to-noise (*S/N*) ratio of the observed spectra. The *g* values were calibrated with an Mn^{2+} marker and the hyperfine coupling (*a*hfc) constants were determined by computer simulation using Calleo ESR Version 1.2 program coded by Calleo Scientific on an Apple Macintosh personal computer.

Results and Discussion

Second-Order Acceleration Effect of NH_4^+ on Rates of Photoinduced Electron-Transfer Reduction of *p*-Benzoquinone in DMSO. Transient absorption spectra of a deaerated DMSO solution of H_2P in the presence of 0.2 M NH_4PF_6 measured at 10 and 200 μs after the laser pulse excitation (515 nm) are shown in Figure 1a, where the triplet−triplet (T−T) absorption band is observed at 440 nm due to $^3H_2P^*$ (* denotes the excited state).[38] The inset shows the triplet decay. Addition of Q (1.0×10^{-3} M) to the $^3H_2P^*$-NH_4PF_6 system results in photoinduced electron transfer from $^3H_2P^*$ to Q to yield $H_2P^{\bullet+}$ (650 nm) and the $Q^{\bullet-}/NH_4^+$ complex (440 nm). The decay of the T−T absorption at 440 nm in the presence of Q becomes much faster than the decay in the absence of Q (compare inset of Figure 1b with that of Figure 1a), which is accompanied by an increase in absorbance at 650 nm due to $H_2P^{\bullet+}$. The absorption band of the $Q^{\bullet-}/NH_4^+$ complex appears in the same wavelength region as the T−T absorption band with a smaller extinction coefficient,[39] as indicated by the residual absorption at 440 nm due to the $Q^{\bullet-}/(NH_4^+)_2$ complex (Figure 1b). Similar photoinduced electron transfer from $^3H_2P^*$ to NQ occurs efficiently in the presence of NH_4PF_6. The occurrence of photoinduced electron transfer is clearly shown by the appearance of the transient absorption band at 650 nm due to $H_2P^{\bullet+}$. The triplet band of H_2P is indeed overlapped with the absorption band due to $Q^{\bullet-}$ and $NQ^{\bullet-}$.

The second-order rate constant (k_{et}) of photoinduced electron transfer from $^3H_2P^*$ to NQ increases parabolically with increasing concentration of NH_4PF_6 as shown in Figure 2 (the k_{et} values

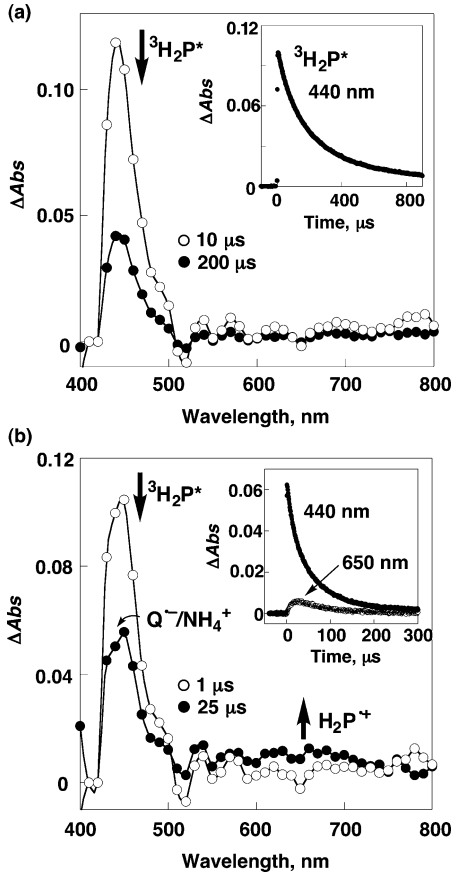

Figure 1. Transient absorption spectra of H_2P (5.0×10^{-5} M) with $[NH_4PF_6] = 0.2$ M (a) in the absence of Q (Inset: time profile at 440 nm) and (b) in the presence of $[Q] = 1.0 \times 10^{-3}$ M (Inset: time profiles at 440 and 650 nm) excited at 515 nm in deaerated DMSO.

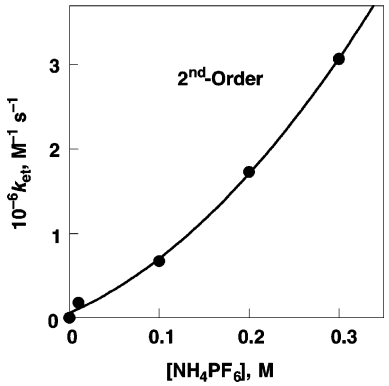

Figure 2. Plot of the second-order rate constant (k_{et}) vs $[NH_4PF_6]$ for photoinduced electron transfer from $^3H_2P^*$ to NQ in the presence of NH_4PF_6 in deaerated DMSO.

are listed in Table 1), where the rate constant of the electron transfer was separated from the dependence of the decay rate constant on quinone concentration.[40] Such a parabolic dependence of k_{et} on concentration of NH_4PF_6 results from formation of a 1:2 complex between $Q^{\bullet-}$ and NH_4^+ (vide infra).

The rate constants of photoinduced electron transfer from $^1H_2P^*$ to NQ were also determined from fluorescence quenching of $^1H_2P^*$ by NQ in the presence of various concentrations of NH_4PF_6 in deaerated DMSO (see the Experimental Section). The k_{et} values are listed in Table 1, where the k_{et} values exhibit a slight increase with increasing concentration of NH_4PF_6, because they are close to being diffusion-limited (2.9×10^9 M^{-1} s^{-1} $\sim$ 4.5×10^9 M^{-1} s^{-1}).

TABLE 1: Driving Force and Rate Constants of Photoinduced Electron Transfer from Singlet or Triplet Excited State of Free-Base Tetraphenylporphyrin to NQ and Q in the Presence of NH_4PF_6 in DMSO

		$^3H_2P^*$		$^1H_2P^*$	
quencher	$[NH_4PF_6]$, M	$-\Delta G_{et}$, eV	k_{et}, M^{-1} s^{-1}	$-\Delta G_{et}$, eV	k_{et}, M^{-1} s^{-1}
NQ	0.002	−0.20	*b*	0.27	
	0.01	−0.09	1.8×10^5	0.38	2.9×10^9
	0.1	−0.02	6.8×10^5	0.45	4.5×10^9
	0.2	(0.02)[a]	1.7×10^6	(0.48)[a,c]	4.4×10^9
	0.3	(0.04)[a]	3.1×10^6	(0.49)[a,c]	4.2×10^9
Q	0.002	0.02		0.49	
	0.01	0.10	2.0×10^7	0.57	4.4×10^9
	0.1	0.16	7.8×10^7	0.63	4.3×10^9
	0.2	(0.20)[a]	1.3×10^8	(0.49)[a,c]	4.6×10^9

[a] Estimated from Nernst plots in Figure 6. [b] Too slow to be determined accurately. [c] Obtained using the E_{ox} values of H_2P in the presence of 0.1 M NH_4PF_6.

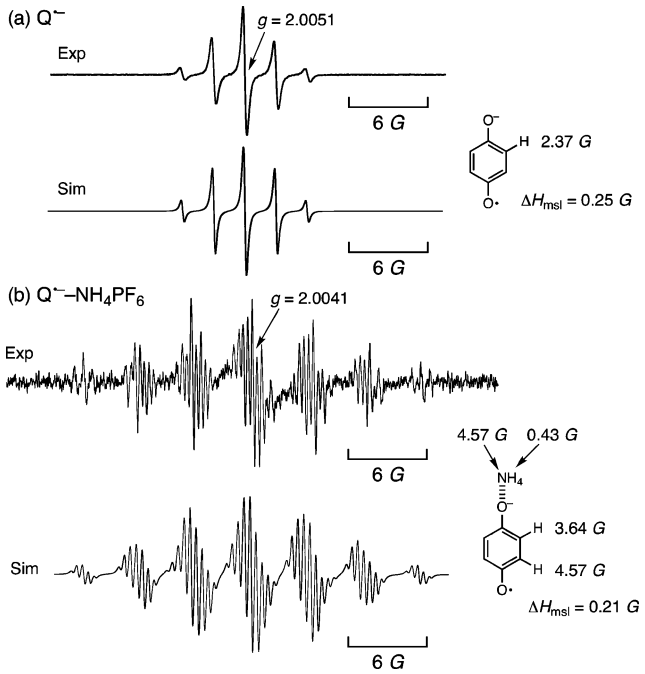

Figure 3. ESR spectra of (a) $Q^{\bullet-}$ generated in the photoirradiation of Q (1.0×10^{-6} M) by $(BNA)_2$ (1.0×10^{-5} M) at 298 K, (b) $Q^{\bullet-}$–NH_4PF_6 complex generated in the photoirradiation of Q (1.0×10^{-4} M) by $(BNA)_2$ (3.0×10^{-4} M) in the presence of NH_4PF_6 (2.0×10^{-3} M) at 333 K (top) with the computer simulation spectra (bottom), the hyperfine coupling constants and the maximum slope line widths (ΔH_{msl}).

ESR Detection of NH_4^+ Complexes with Semiquinone Radical Anions. The $Q^{\bullet-}/NH_4^+$ complex is successfully detected by ESR in photoinduced electron transfer from dimeric 1-benzyl-1,4-dihydronicotinamide $[(BNA)_2]$ to Q in the presence of NH_4PF_6 in DMSO at 298 K. The $(BNA)_2$ is known to act as a unique electron donor to produce the radical anions of electron acceptors.[37b] The ESR spectrum of $Q^{\bullet-}$ in the absence of NH_4PF_6 at $g = 2.0051$ with hyperfine splitting due to four equivalent protons of $Q^{\bullet-}$ [a(4H) = 2.37 G] in Figure 3a (the computer simulation spectrum is also shown together with the observed spectrum) is drastically changed to the spectrum at $g = 2.0041$ in the presence of 2.0×10^{-3} M NH_4PF_6 in DMSO at 333 K as shown in Figure 3b.[41] The observed ESR spectrum consists of the superhyperfine splitting due to four equivalent protons [a(4H) = 0.43 G] and one nitrogen [a(N) = 4.57 G] of NH_4^+ in addition to the hyperfine splitting due to two sets of

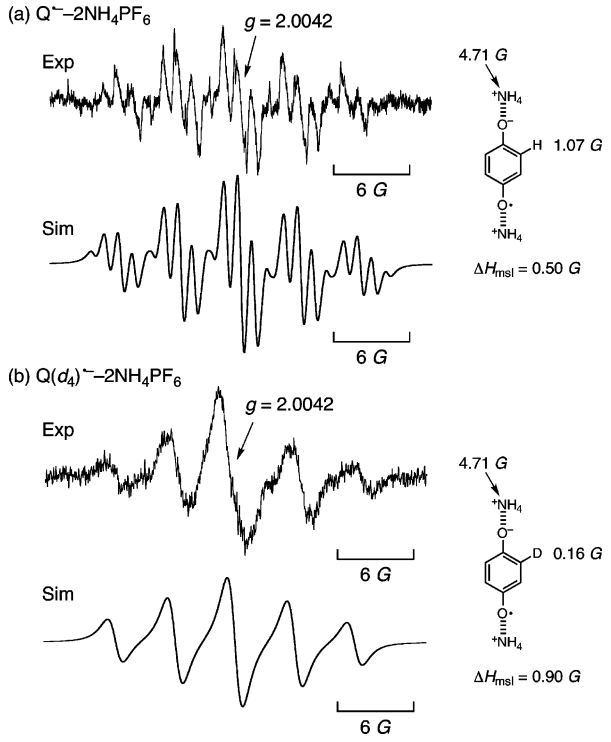

Figure 4. ESR spectra of (a) the $Q^{\bullet-}-2NH_4PF_6$ complex generated in the photoirradiation of Q (1.0×10^{-4} M) by $(BNA)_2$ (3.0×10^{-4} M) in the presence of NH_4PF_6 (5.0×10^{-2} M) in deaerated DMSO at 298 K and (b) the tetradeuterated $Q^{\bullet-}-2NH_4PF_6$ complex generated in the photoirradiation of Q-d_4 (1.0×10^{-6} M) by $(BNA)_2$ (1.0×10^{-5} M) in the presence of NH_4PF_6 (5.0×10^{-2} M) in deaerated DMSO at 298 K (top) with the computer simulation spectra (bottom), the hyperfine coupling constants, and the maximum slope line widths (ΔH_{msl}).

two equivalent protons of $Q^{\bullet-}$ [a(2H) = 3.64 G, 4.57 G]. These hyperfine and superhyperfine splitting constants are determined by the computer simulation spectrum which agrees well with the observed spectrum (Figure 3b). The observation of the superhyperfine structure due to NH_4^+ and two different a(2H) values clearly indicates that NH_4^+ forms the 1:1 complex with $Q^{\bullet-}$ and that no proton transfer occurs from NH_4^+ to $Q^{\bullet-}$ to produce $QH^{\bullet}$.

When the concentration of NH_4PF_6 is increased to 1.0×10^{-2} M, the ESR spectrum is changed to that shown in Figure 4a, which consists of hyperfine splitting due to four equivalent protons of $Q^{\bullet-}$ [a(4H) = 1.07 G] and superhyperfine splitting due to two equivalent nitrogens of NH_4^+ [a(2N) = 4.71 G] as indicated by the agreement with the computer simulation spectrum. This indicates formation of the 1:2 complex between $Q^{\bullet-}$ and NH_4^+: $Q^{\bullet-}/(NH_4^+)_2$. The superhyperfine splittings due to eight equivalent protons are not observed probably due to the larger line width. Deuterium substitution of four hydrogen atoms of Q results in a change in the splitting pattern from the spectrum in Figure 4a to that in Figure 4b, where Q is substituted by *p*-benzoquinone-d_4. The computer simulation spectrum using the same hyperfine coupling (hfc) constant values except for the deuterium (a(4D) = 0.16 G), which are reduced by a factor of 0.153, agrees well with the observed ESR spectrum of the $Q^{\bullet-}/(NH_4^+)_2$ complex (Figure 4b). Such an agreement confirms the hfc assignment in Figure 4a. The observed small a(4H) values and large a(2N) values clearly indicate the existence of orbital interaction, i.e., hydrogen bonding between $Q^{\bullet-}$ and two NH_4^+ cations in addition to the electrostatic interaction in the $Q^{\bullet-}/(NH_4^+)_2$ complex.

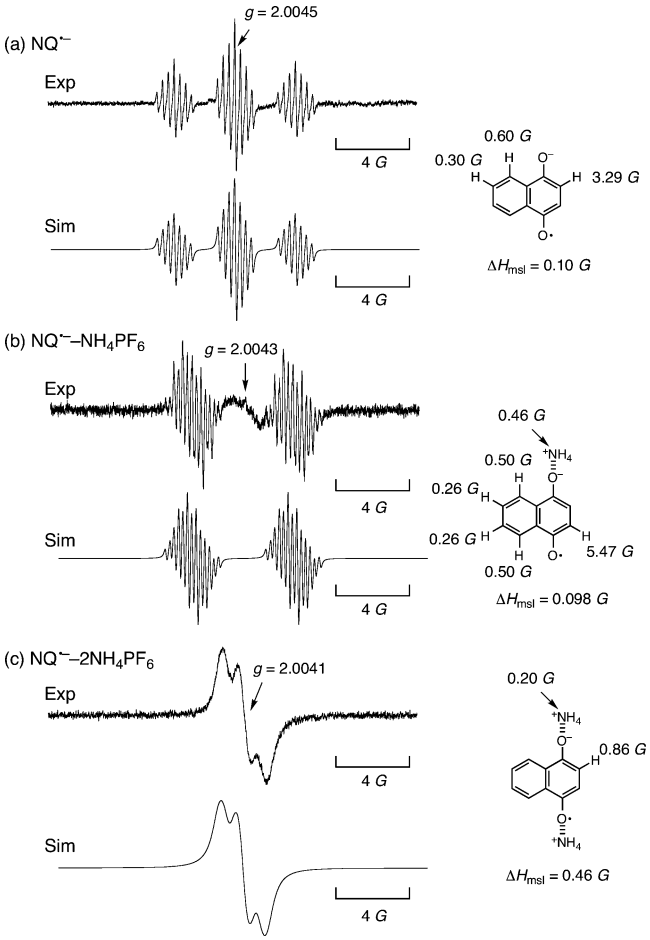

Figure 5. ESR spectra of (a) $NQ^{\bullet-}$ generated in the photoirradiation of NQ (1.0×10^{-6} M) by $(BNA)_2$ (1.0×10^{-5} M) at 298 K, (b) the $NQ^{\bullet-}-NH_4PF_6$ complex generated in the photoirradiation of NQ (2.0×10^{-4} M) by $(BNA)_2$ (3.0×10^{-3} M) in the presence of NH_4PF_6 (5.0×10^{-3} M) at 333 K, and (c) the $NQ^{\bullet-}-2NH_4PF_6$ complex generated in the photoirradiation of NQ (2.0×10^{-3} M) by $(BNA)_2$ (3.0×10^{-3} M) in the presence of NH_4PF_6 (0.1 M) in deaerated DMSO at 298 K (top) with the computer simulation spectra (bottom), the hyperfine coupling constants, and the maximum slope line widths (ΔH_{msl}).

The ESR spectrum of $NQ^{\bullet-}$ (Figure 5a) is also changed significantly in the presence of NH_4PF_6 to those of the $NQ^{\bullet-}/NH_4^+$ complex and $NQ^{\bullet-}/(NH_4^+)_2$ complex depending on the concentration of NH_4PF_6 as shown in Figure 5, parts b and c, respectively. The comparison of the observed spectra with the computer simulation spectra affords the hyperfine and superhyperfine splitting constants (Figure 5).

Effect of NH_4^+ on One-Electron Reduction Potentials of Quinones in DMSO. Significant positive shifts of the one-electron reduction potentials (E_{red}) of Q and NQ are observed in the presence of NH_4PF_6 as compared with those in the presence of NBu_4PF_6. This is shown in Figure 6, where E_{red} determined from the cyclic voltammetry measurements in DMSO are plotted against log[electrolyte]. The slopes of the plot of E_{red} for $Q/Q^{\bullet-}$ and $NQ/NQ^{\bullet-}$ vs log[NH_4PF_6] are the same (0.12 V), whereas the slope of the plot of E_{red} of $Q/Q^{\bullet-}$ vs log[NBu_4PF_6] is only 0.026 V. The slope of 0.12 V is twice the expected slope (2.3RT/F at 298 K) by the Nernst equation (eq 2) for a 1:1 complex formation between $Q^{\bullet-}$ (or $NQ^{\bullet-}$) and NH_4^+.

E_{red} is given as a function of concentration of NH_4PF_6, in accordance with the Nernst equation (eq 2) for a 1:1 complex formation between $Q^{\bullet-}$ (or $NQ^{\bullet-}$) and NH_4^+, where E^0_{red} is the one-electron reduction potential in the absence of NH_4PF_6, K_{red}

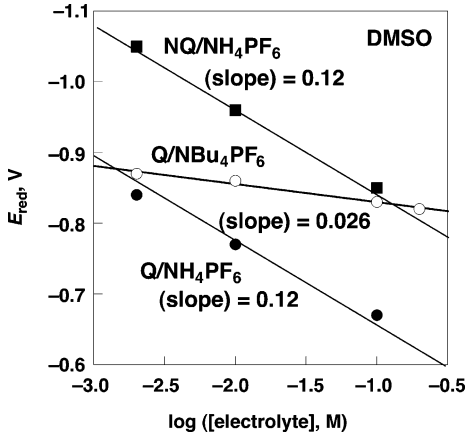

Figure 6. Nernst plots of E_{red} for Q or NQ against log[electrolyte]; NQ/NH_4PF_6 (■), Q/NBu_4PF_6 (○), Q/NH_4PF_6 (●) in deaerated DMSO.

is the formation constant of the $Q^{\bullet-}/NH_4^+$ ($NQ^{\bullet-}/NH_4^+$) complex, and K_{ox} is the formation constant of the Q/NH_4^+ (NQ/NH_4^+) complex.[42]

$$E_{red} = E^0_{red} + (2.3RT/F)\log\{(1 + K_{red}[NH_4PF_6])/(1 + K_{ox}[NH_4PF_6])\} \quad (2)$$

Since $K_{red}[NH_4PF_6] \gg 1$ and $K_{ox}[NH_4PF_6] \ll 1$, eq 2 can be written as shown in eq 3

$$E_{red} = E^0_{red} + (2.3RT/F)\log K_{red}[NH_4PF_6] \quad (3)$$

In a 1:2 complex formation between $Q^{\bullet-}$ (or $NQ^{\bullet-}$) and $2NH_4^+$, eq 3 is written as shown by eq 4, where $K_{red(2)}$ is the formation constant of the $Q^{\bullet-}/(NH_4^+)_2$ [$NQ^{\bullet-}/(NH_4^+)_2$] complex.[42] When $K_{red(2)}[NH_4PF_6] \gg 1$, the slope of the Nernst plot is expected to be 0.12, and this is observed experimentally in Figure 6. This indicates that $Q^{\bullet-}$ or $NQ^{\bullet-}$ forms a complex with two equivalents of NH_4^+.

$$E_{red} = E^0_{red} + (2.3RT/F)\log(K_{red}[NH_4PF_6] + K_{red}K_{red(2)}[NH_4PF_6]^2) \quad (4)$$

The slope of the Nernst plot (0.12) in Figure 6 agrees both with a parabolic dependence of k_{et} on concentration of NH_4PF_6 and also with the ESR spectra in Figures 4 and 5c, indicating formation of a 1:2 complex between $Q^{\bullet-}$ (or $NQ^{\bullet-}$) and NH_4^+.

The driving force of electron transfer from $^1H_2P^*$ or $^3H_2P^*$ to Q or NQ in the presence of various concentrations of NH_4PF_6 were determined as listed in Table S1 (Supporting Information).

Accelerating Effect of NBu_4^+ on Rates of Photoinduced Electron-Transfer Reduction of Quinones in CH_2Cl_2. When NH_4PF_6 was replaced by NBu_4PF_6, no acceleration effect of NBu_4PF_6 (at least up to 0.2 M) was observed in photoinduced electron transfer from $^3H_2P^*$ to Q in DMSO.[43] In a less polar solvent such as CH_2Cl_2, however, NBu_4PF_6 shows a remarkable acceleration effect on the photoinduced electron-transfer reaction. Transient absorption spectra of a deaerated CH_2Cl_2 solution of H_2P in the presence of 0.1 M NBu_4PF_6 are shown in Figure 7a. Photoinduced electron transfer from $^3H_2P^*$ to Q in the presence of NBu_4PF_6 occurs efficiently in CH_2Cl_2 to produce $H_2P^{\bullet+}$ and the $Q^{\bullet-}/NBu_4^+$ complex as shown in Figure 7b.

Decay rates of the T−T absorption of $^3H_2P^*$ in the presence of Q (or NQ) obey pseudo-first-order kinetics, and the pseudo-first-order rate constant increases linearly with increasing concentration of Q (or NQ). The second-order rate constants of

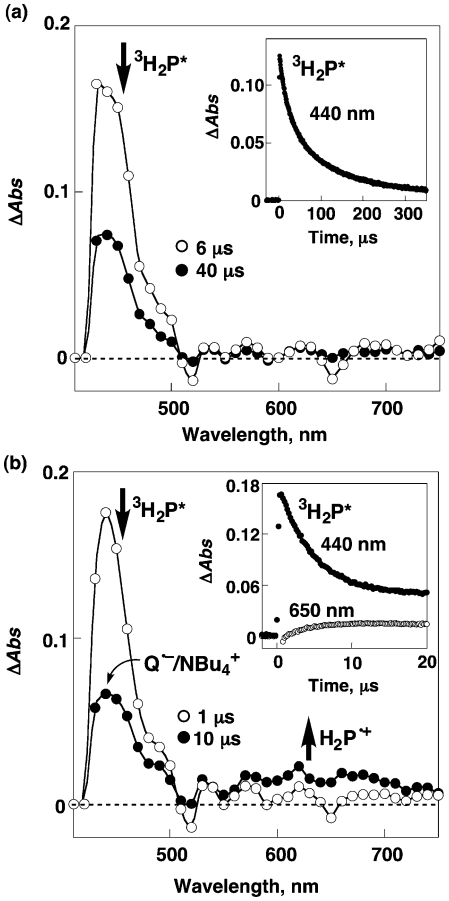

Figure 7. Transient absorption spectra of H_2P (1.0×10^{-5} M) with $[NBu_4PF_6] = 0.1$ M (a) in the absence of Q (Inset: time profile at 440 nm) and (b) in the presence of $[Q] = 1.0 \times 10^{-3}$ M (Inset: time profiles at 440 and 650 nm) excited at 515 nm in deaerated CH_2Cl_2.

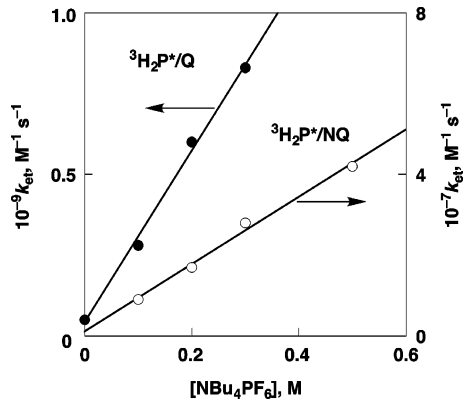

Figure 8. Plots of the second-order rate constant (k_{et}) vs $[NBu_4PF_6]$ for photoinduced electron transfer from $^3H_2P^*$ to Q or NQ in deaerated CH_2Cl_2.

photoinduced electron transfer (k_{et}) were determined from the slopes of linear plots of pseudo-first-order rate constants vs concentration of Q and NQ. The k_{et} values increase linearly with increasing concentration of NBu_4PF as shown in Figure 8 (the data are listed in Table 2 with the driving force of electron transfer from $^3H_2P^*$ to Q).

The rate constants of photoinduced electron transfer from the singlet excited state of H_2P ($^1H_2P^*$) to NQ were also determined from fluorescence quenching of $^1H_2P^*$ by NQ in the presence of various concentrations of NBu_4PF_6 in deaerated CH_2Cl_2 (see the Supporting Information Figure S1). The fluorescence of H_2P is quenched by electron transfer from $^1H_2P^*$ to NQ. The rate

TABLE 2: Driving Force and Rate Constants of Electron Transfer from Singlet and Triplet Excited States of Free-Base Tetraphenylporphyrin ($^1H_2P^*$ and $^3H_2P^*$) to Q and NQ in the Absence and Presence of NBu_4PF_6 in CH_2Cl_2

		$^3H_2P^*$		$^1H_2P^*$	
quencher	$[NBu_4PF_6]$, M	$-\Delta G_{et}$, eV	k_{et}, $M^{-1}\,s^{-1}$	$-\Delta G_{et}$, eV	k_{et}, $M^{-1}\,s^{-1}$
NQ	0		*b*		8.2×10^9
	0.002	−0.35	*b*	0.12	$(8.2 \times 10^9)^c$
	0.1	−0.25	9.0×10^6	0.22	8.3×10^9
	0.2	−0.21	1.7×10^7	0.26	8.4×10^9
	0.3	$(-0.20)^a$	2.8×10^7	$(0.27)^a$	8.8×10^9
	0.5	$(-0.19)^a$	4.2×10^7	$(0.28)^a$	9.0×10^9
Q	0		5.0×10^7		1.1×10^{10}
	0.002	−0.15	$(5.0 \times 10^7)^c$	0.32	$(1.1 \times 10^{10})^c$
	0.1	−0.07	2.8×10^8	0.40	1.0×10^{10}
	0.2	−0.03	6.0×10^8	0.44	1.1×10^{10}
	0.3	$(-0.02)^a$	8.3×10^8	$(0.45)^a$	1.1×10^{10}

[a] Estimated from Nernst plots in Figure 12. [b] Too slow to be determined accurately. [c] Values in the absence of NBu_4PF_6.

constants of the fluorescence quenching by the photoinduced electron transfer (k_{et}) were determined using the Stern−Volmer plots (Figure S1), where the lifetime of H_2P in CH_2Cl_2 is determined as $\tau = 10.8$ ns. The k_{et} values are listed in Table 2, where the k_{et} values are constant irrespective of variation of concentration of NBu_4PF_6, because they are already diffusion-limited ($8.2 \times 10^9 \sim 9.0 \times 10^9\ M^{-1}\,s^{-1}$).

The $Q^{\bullet-}/NBu_4^+$ complex is detected by ESR measurements after photoinduced electron transfer from $(BNA)_2$ to Q in the presence of NBu_4PF_6 in CH_2Cl_2 at 298 K. The ESR spectrum of $Q^{\bullet-}$ in the presence of NBu_4PF_6 in CH_2Cl_2 exhibits the signal at $g = 2.0043$ and has a hyperfine splitting constant due to four equivalent protons [$a(4H) = 2.39$ *G*], which agrees with the spectrum in the absence of NBu_4PF_6 (see the Supporting Information Figure S2). This indicates that the interaction between $Q^{\bullet-}$ and NBu_4^+ is largely electrostatic rather than being due to covalent bonding which would affect the spin distribution of $Q^{\bullet-}$.

The one-electron reduction potentials (E_{red}) of quinones were determined by cyclic voltammetry using a microelectrode (∼10 μm diam; see the Experimental Section) in the presence of various concentrations of NBu_4PF_6 in CH_2Cl_2. The cyclic voltammogram of *p*-benzoquinone (Q) exhibits the one-electron redox couple corresponding to $Q/Q^{\bullet-}$ in CH_2Cl_2 as shown in Figure 9, where the redox potentials (vs Fc^+/Fc) are shifted in a positive direction with increasing concentration of NBu_4PF_6 (Table 3). The E_{red} value of Q in CH_2Cl_2 containing 0.50 M NBu_4PF_6 (−0.89 V vs Fc^+/Fc) is more positive by 0.17 V than in the presence of 2.0×10^{-3} M NBu_4PF_6 (−1.06 V vs Fc^+/Fc). Such a positive shift of 0.17 V corresponds to 750 times enhancement in terms of the rate constant of electron transfer, provided that the change in the thermodynamics due to the difference in concentration of NBu_4PF_6 is directly reflected in the rate of electron transfer.[44] Similar positive shifts of E_{red} are observed in the case of $NQ/NQ^{\bullet-}$ couple with increasing concentration of NBu_4PF_6 (Table 3). In contrast, the one-electron oxidation potential (vs Fc^+/Fc) of free-base tetraphenylporphyrin (H_2P) corresponding to the $H_2P^{\bullet+}/H_2P$ couple in CH_2Cl_2 remains virtually the same with changes in concentration of NBu_4PF_6. This is shown in Figure 10 and Table 3.

Positive shifts of E_{red} for Q and NQ with increasing concentration of NBu_4PF_6 are also observed in PhCN, MeCN, and DMSO, where the effects of NBu_4PF_6 on E_{red} decrease with increasing the solvent polarity; that is, the ΔE_{red} for $Q/Q^{\bullet-}$ couple between concentration of 0.002 and 0.2 M electrolyte is

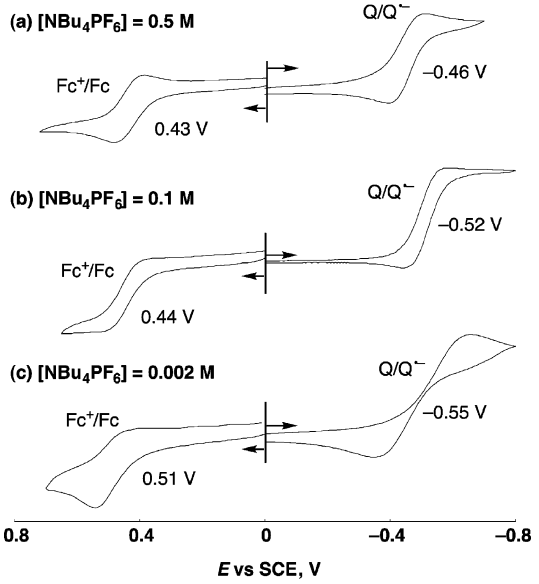

Figure 9. Cyclic voltammograms of *p*-benzoquinone (Q) (1.0×10^{-3} M) in the presence of (a) $[NBu_4PF_6] = 0.5$ M, (b) 0.1 M, and (c) 0.002 M in deaerated CH_2Cl_2 determined by using a ∼10 μm diam Pt disk microelectrode as a working electrode.

140 mV in CH_2Cl_2, 70 mV in PhCN, 80 mV in MeCN, and 50 mV in DMSO (Table 3). On the other hand, virtually no potential shifts in E_{red} or E_{ox} values with variation of concentration of NBu_4PF_6 are observed in the case of $HV^{2+}/HV^{\bullet+}$, Ru^{2+}/Ru^+, or $H_2P^{\bullet+}/H_2P$ (Table 3). The one-electron oxidation potentials for $ZnP^{\bullet+}/ZnP$ and Ru^{3+}/Ru^{2+} are shifted to the negative and positive directions, respectively, with increasing concentration of NBu_4PF_6. The Zn^{2+} ion of ZnP may interact with the counteranion of the supporting electrolyte, which results in stabilization of $ZnP^{\bullet+}$ due to counteranion ligation as indicated by Moore and co-workers.[32]

The counter anion effects on the redox potentials were also examined using three different kinds of counteranions, i.e., PF_6^-, ClO_4^-, and Br^-, all with the countercation NBu_4^+. The E_{red} of the $Q/Q^{\bullet-}$ and $NQ/NQ^{\bullet-}$ couples in deaerated MeCN were determined from the cyclic voltammetry measurements and plots of E_{red} vs log[electrolyte], electrolyte = NBu_4PF_6, NBu_4ClO_4, and NBu_4Br, are shown in Figure 11a. The E_{red} values are virtually the same irrespective of the difference in the counteranions. On the other hand, plots of E_{red} values for $HV^{2+}/HV^{\bullet+}$ vs log[electrolyte], electrolyte = NBu_4PF_6, NBu_4ClO_4, and NBu_4Br, show only random shifts with changes in the type of counteranions and concentration of the NBu_4^+ salts (Figure 11b).[45] Since the counteranion has no effect on the E_{red} values of Q and NQ (Figure 11a), the positive shifts of E_{red} with increasing concentration of NBu_4PF_6 (Table 3) are ascribed to the interaction of NBu_4^+ with $Q^{\bullet-}$ and $NQ^{\bullet-}$, respectively.

The free energy change of electron transfer (ΔG_{et}) from H_2P to Q and NQ in the presence of NBu_4PF_6 is given by eq 5, where ΔG_{et}^0 is the free energy change of electron transfer in the absence of NBu_4PF_6, which is obtained by eq 6 (*e* stands for the elementary charge).

$$\Delta G_{et} = \Delta G_{et}^0 - (2.3RT/F) \log K_{red}[NBu_4PF_6] \qquad (5)$$

$$\Delta G_{et} = e(E_{ox} - E_{red}) \qquad (6)$$

The Nernst plots of ΔG_{et} vs log[NBu_4PF_6] in CH_2Cl_2 and PhCN are shown in Figure 12 (parts a and b, respectively). The

TABLE 3: One-Electron Redox Potentials of *p*-Benzoquinone (Q), 1,4-Naphthoquinone (NQ), Hexyl Viologen (HV^{2+}), $Ru(bpy)_3^{2+}$, H_2P, and ZnP in the Presence of NBu_4PF_6 in CH_2Cl_2, PhCN, MeCN, and DMSO

		E_{red} vs Fc^+/Fc, V				E_{ox} vs Fc^+/Fc, V		
solvent	$[NBu_4PF_6]$, M	$Q/Q^{\bullet-}$	$NQ/NQ^{\bullet-}$	$HV^{2+}/HV^{\bullet+}$	Ru^{2+}/Ru^+	$H_2P^{\bullet+}/H_2P$	$ZnP^{\bullet+}/ZnP$	Ru^{3+}/Ru^{2+}
CH_2Cl_2	0.002	−1.06	−1.26	−0.73		0.52	0.29	
	0.01	−1.02	−1.20	−0.72		0.52	0.29	
	0.1	−0.96	−1.14	−0.73		0.54	0.30	
	0.2	−0.92	−1.10	−0.73		0.54	0.31	
	0.5	−0.89	−1.07	——		——	——	
PhCN	0.002	−1.02	−1.21	−0.75		0.55	0.32	
	0.01	−0.99	−1.18	−0.78		0.55	0.32	
	0.1	−0.97	−1.15	−0.79		0.55	0.34	
	0.2	−0.95	−1.14	−0.78		0.56	0.36	
MeCN	0	−1.00	−1.20	−0.84	−1.72			n.d.
	0.002	−0.97	−1.14	−0.82	−1.71			0.95
	0.01	−0.96	−1.11	−0.81	−1.71			0.91
	0.1	−0.92	−1.09	−0.81	−1.70			0.86
	0.2	−0.89	−1.07	−0.82	−1.71			0.85
	0.5	−0.85	−1.04	−0.84	——			——
DMSO	0.002	−0.87		−0.90				
	0.01	−0.86		−0.89				
	0.1	−0.83		−0.89				
	0.2	−0.82		−0.89				

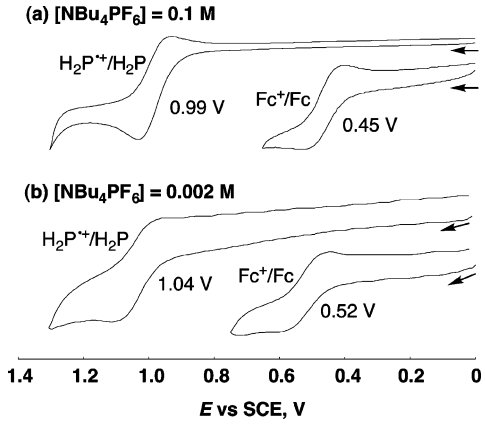

Figure 10. Cyclic voltammograms of free-base porphyrin (H_2P) (1.0×10^{-3} M) in the presence of (a) $[NBu_4PF_6] = 0.1$ M and (b) 0.002 M in deaerated CH_2Cl_2 determined by using a 3 mm diam glassy carbon electrode as a working electrode due to small currents.

slope of each plot in CH_2Cl_2 was determined to be −0.059, which agrees with the expected slope ($-2.3RT/F$ at 298 K) by the Nernst equation (eq 4) for formation of a 1:1 complex between $Q^{\bullet-}$ ($NQ^{\bullet-}$) and NBu_4^+.[46] The slope (−0.025) of each plot in PhCN is smaller than that in CH_2Cl_2 and this might result from the weaker binding between $Q^{\bullet-}$ ($NQ^{\bullet-}$) and NBu_4^+ in the higher polar solvent.

Large positive shifts of E_{red} of Q and NQ in CH_2Cl_2 together with constant E_{ox} values of H_2P with variation of concentration of NBu_4^+ result in an enhancement of the photoinduced electron transfer from the excited states of H_2P to Q and NQ.

Driving Force Dependence of Rate Constants of Photoinduced Electron Transfer in the Presence of NBu_4PF_6 and NH_4PF_6. Photoinduced electron transfer from singlet or triplet excited state of H_2P to Q or NQ may occur as shown in eq 7

$$H_2TPP^* + Q \underset{k_{21}}{\overset{k_{12}}{\rightleftharpoons}} (H_2TPP^*\ Q) \xrightarrow[+NR_4PF_6]{k_{ET}} H_2TPP^{\bullet+} + Q^{\bullet-}/NR_4PF_6 \qquad R = Bu, H \quad (7)$$

(illustrated in the case of Q), where k_{12} and k_{21} are diffusion and dissociation rate constants in the encounter complex (H_2P^* Q) and k_{ET} is the rate constants of the intracomplex electron transfer from H_2P^* to Q. The observed second-order rate constant (k_{et}) of photoinduced electron transfer is given by eq 8. The driving force dependence of log k_{ET} for adiabatic outer-sphere electron transfer has well been established by Marcus as given by eq 9, where k_B is the Boltzmann constant

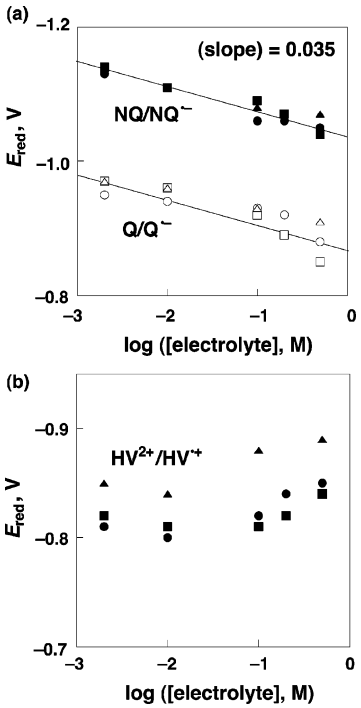

Figure 11. (a) Nernst plots of E_{red} for Q or NQ against log[electrolyte], electrolyte = NBu_4PF_6 (■ and □), NBu_4ClO_4 (● and ○), and NBu_4Br (▲ and △), in deaerated MeCN. (b) Nernst plots of E_{red} for HV^{2+} against log[electrolyte], electrolyte = NBu_4PF_6 (■), NBu_4ClO_4 (●), NBu_4Br (▲), in deaerated MeCN.

$$k_{et} = k_{ET}k_{12}/(k_{ET} + k_{21}) \quad (8)$$

$$k_{ET} = (k_BT/h)\exp(-(\Delta G_{et} + \lambda)^2/4\lambda k_BT) \quad (9)$$

h is Plank constant and λ is the reorganization energy of electron

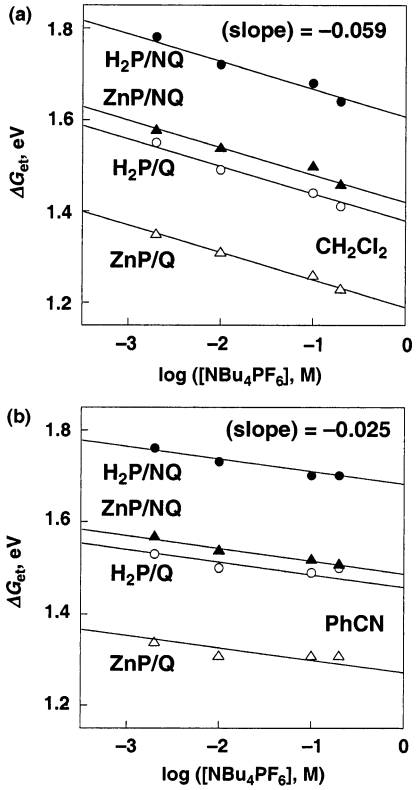

Figure 12. Nernst plots of ΔG_{et} vs log[NBu_4PF_6] (a) in deaerated CH_2Cl_2 and (b) in deaerated PhCN.

transfer. From eqs 8 and 9 is derived eq 10 where Z (= $(k_BT/h)(k_{12}/k_{21})$) is the collision frequency for an intermolecular reaction which is taken as 1×10^{11} M^{-1} s^{-1}.[47] The k_{12} values in CH_2Cl_2 and DMSO are taken as 1.1×10^{10} and 7.0×10^9 M^{-1} s^{-1}, respectively.[48]

$$k_{et} = \frac{k_{12}Z \exp\left(-\dfrac{(\Delta G_{et} + \lambda)^2}{4\lambda k_B T}\right)}{k_{12} + Z \exp\left(-\dfrac{(\Delta G_{et} + \lambda)^2}{4\lambda k_B T}\right)} \qquad (10)$$

Figure 13 shows the driving force dependence of log k_{et} in CH_2Cl_2 and DMSO, where the k_{et} and $-\Delta G_{et}$ values are taken from Tables 1 and 2. The log k_{et} values increase with an increase in the $-\Delta G_{et}$ values to reach a diffusion rate constant as the photoinduced electron transfer becomes energetically favorable.

The driving force dependence of k_{et} is well reproduced using eq 10 as indicated by the line in Figure 13, where the λ values are taken as 0.40 eV in CH_2Cl_2 and 1.05 eV in DMSO. This indicates that the change in k_{et} with variation of concentration of ammonium ions (NBu_4^+ and NH_4^+) results from the change in the driving force due to the complex formation of $Q^{\bullet-}$ and $NQ^{\bullet-}$ with NBu_4^+ and NH_4^+ in accordance with the Marcus theory of electron transfer and that the λ value remains constant with variation of concentrations of NBu_4^+ and NH_4^+. The larger λ value in DMSO as compared to the value in CH_2Cl_2 is ascribed to the larger solvent reorganization energy in the more polar solvent (DMSO). The constant λ value with variation of concentration of ammonium cations in ammonium ion-promoted photoinduced electron transfer from the excited states of H_2P to Q or NQ (Figure 13) sharply contrasts with the case of metal ion-promoted electron-transfer reactions in which the reorganization energy (λ = 2.20 eV) is much larger and the λ value decreases with increasing concentration of metal ions.[17b]

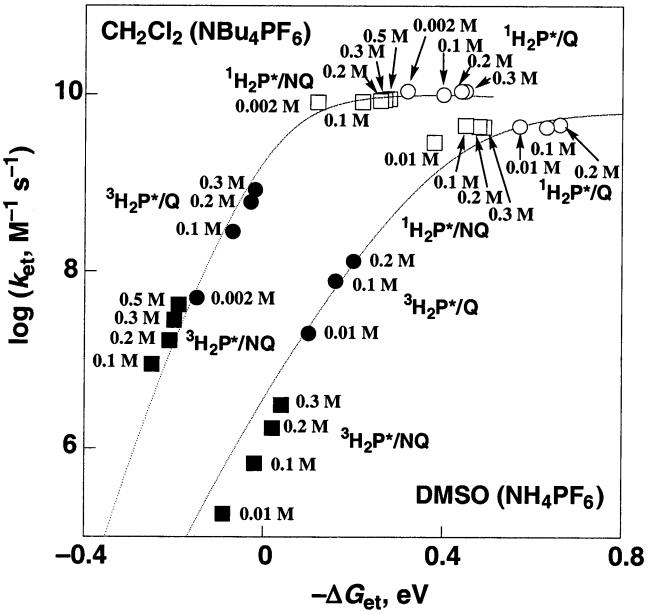

Figure 13. Driving force ($-\Delta G_{et}$) dependence of log k_{et} for photoinduced electron transfer from singlet and triplet excited states of H_2P to Q and NQ in the presence of NBu_4PF_6 in deaerated CH_2Cl_2 and in the presence of NH_4PF_6 in deaerated DMSO at 298 K. The lines represent the fits to eq 10 with λ = 0.40 eV in CH_2Cl_2 and λ = 1.05 eV in DMSO.

Such a difference comes from the relatively weak binding of $Q^{\bullet-}$ and $NQ^{\bullet-}$ with NBu_4^+ and NH_4^+ as compared with the strong binding with metal ions which act as Lewis acids.[17b]

In conclusion, the electrostatic complex formation between quinone radical anions and NBu_4^+ in CH_2Cl_2 results in a positive shift of the one-electron reduction potentials of the quinones, leading to a significant enhancement of the rates of photoinduced electron transfer-reduction involving the quinones. Such an interaction between quinone radical anions and NBu_4^+ is largely diminished in a polar solvent (DMSO). However, complex formation between the quinone radical anions and two-equivalents of NH_4^+ through hydrogen bonding also results in a large positive shift in the one-electron reduction potentials of the quinones, leading to a significant enhancement in the rates of photoinduced electron transfer-reduction of quinones, even in DMSO. The driving force dependence of the observed rate constants for photoinduced electron transfer from porphyrins to quinones with large variation of ammonium ion concentration is well evaluated in light of the Marcus theory of electron transfer.[33] Large effects of ammonium ions on the one-electron reduction potentials of quinones and the rates of their electron-transfer reduction, particularly through hydrogen bonding, provide valuable insights into the versatile important role of ammonium ions in the biological redox reactions, including the photosynthetic reaction center.

Acknowledgment. This work was partially supported by a Grant-in-Aid (13440216) from the Ministry of Education, Culture, Sports, Science and Technology, Japan, the Robert A. Welch Foundation (K.M.K., Grant E−680), and the Texas Advanced Research program to K.M.K. under Grant No. 003652-0018-2001. K.O. acknowledges a 21st Century COE program of Osaka University for financial support during his stay at University of Houston.

Supporting Information Available: Redox potentials in the presence of NBu_4ClO_4 and NBu_4Br in MeCN and NH_4PF_6 in

DMSO (Table S1), fluorescence spectra of H_2P in the presence of various concentrations of NQ in CH_2Cl_2 and Stern−Volmer plot (Figure S1), and ESR spectra of $Q^{\bullet-}$ in CH_2Cl_2 in the absence and presence of NBu_4PF_6 (Figure S2). This material is available free of charge via the Internet at http://pubs.acs.org.

References and Notes

(1) Kaim, W.; Schwederski, B. *Bioinorganic Chemistry: Inorganic Elements in the Chemistry of Life*; Wiley: Chichester, U.K., 1994.

(2) *Principles of Bioinorganic Chemistry*; Lippard, S. J., Berg, J. M., Eds.; University Science Books: Mill Valley, CA, 1994.

(3) Fukuzumi, S.; Ohtsu, H.; Ohkubo, K.; Itoh, S.; Imahori, H. *Coord. Chem. Rev.* **2002**, *226*, 71.

(4) (a) Limburg, J.; Szalai, V. A.; Brudvig, G. W. *J. Chem. Soc., Dalton Trans*. **1999**, 1353. (b) Einsle, O.; Messerschmidt, A.; Stach, P.; Bourenkov, G. P.; Bartunik, H. D.; Huber, R.; Kroneck, P. M. H. *Nature* **1999**, *400*, 476.

(5) (a) Riistama, S.; Laakkonen, L.; Wikström, M.; Verkhovsky, M. I.; Puustinen, A. *Biochemistry* **1999**, *38*, 10670. (b) Xia, Z.-x.; Dai, W.-w.; Zhang, Y.-f.; White, S. A.; Boyd, G. D.; Mathews, F. S. *J. Mol. Biol.* **1996**, *259*, 480.

(6) Ghosh, M.; Anthony, C.; Harlos, K.; Goodwin, M. G.; Blake, C. *Structure* **1995**, *3*, 177.

(7) (a) Itoh, S.; Kawakami, H.; Fukuzumi, S. *J. Am. Chem. Soc*. **1997**, *119*, 439. (b) Itoh, S.; Kawakami, H.; Fukuzumi, S. *Biochemistry* **1998**, *37*, 6562. (c) Itoh, S.; Taniguchi, M.; Takada, N.; Nagatomo, S.; Kitagawa, T.; Fukuzumi, S. *J. Am. Chem. Soc.* **2000**, *122*, 12087. (d) Itoh, S.; Kumei, H.; Nagatomo, S.; Kitagawa, T.; Fukuzumi, S. *J. Am. Chem. Soc.* **2001**, *123*, 2165.

(8) (a) Fukuzumi, S.; Itoh, S. *Antioxid. Redox Signaling* **2001**, *3*, 807. (b) Itoh, S.; Taki, M.; Fukuzumi, S. *Coord. Chem. Rev.* **2000**, *198*, 3.

(9) (a) Bruhn, H.; Nigam, S.; Holzwarth, J. F. *Faraday Discuss. Chem. Soc.* **1982**, *74*, 129. (b) Santamaria, J. In *Photoinduced Electron Transfer*; Fox, M. A., Chanon, M., Eds.; Elsevier: Amsterdam, 1988; Part B, pp 483−540. (c) Galan, M.; Dominguez, M.; Andreu, R.; Moya, M. L.; Sanchez, F.; Burgess, J. *J. Chem. Soc., Faraday Trans.* **1990**, *86*, 937.

(10) (a) Sivaguru, J.; Natarajan, A.; Kaanumalle, L. S.; Shailaja, J.; Uppili, S.; Joy, A.; Ramamurthy, V. *Acc. Chem. Res.* **2003**, *36*, 509. (b) Ramamurthy, V.; Robbins, R. J.; Thomas, K. J.; Lakshminarasimhan, P. H. In *Molecular Solid State*; Whitsell, J. K., Ed.; John Wiley & Sons Ltd.: Chichester, U.K., 1999; pp 63−140.

(11) (a) Fukuzumi, S. In *Advances in Electron-Transfer Chemistry*; Mariano, P. S., Ed.; JAI Press: Greenwich, CT, 1992; Vol. 2, pp 67−175. (b) Fukuzumi, S. *Bull. Chem. Soc. Jpn.* **1997**, *70*, 1. (c) Fukuzumi, S.; Itoh, S. In *Advances in Photochemistry*; Neckers, D. C., Volman, D. H., von Bünau, G., Eds.; Wiley: New York, 1999; Vol. 25, pp 107−172.

(12) (a) Fukuzumi, S. In *Electron Transfer in Chemistry*; Balzani, V., Ed.; Wiley-VCH: Weinheim, Germany, 2001; Vol. 4, pp 3−67. (b) Fukuzumi, S. *Org. Biomol. Chem.* **2003**, *1*, 609. (c) Fukuzumi, S.; Imahori, H. In *Photochemistry of Organic Molecules in Isotropic and Anisotropic Media*; Ramamurthy, V., Schanze, K. S., Eds.; Marcel Delkker: New York, 2003; pp 227−273.

(13) (a) Goodson, B.; Schuster, G. B. *Tetrahedron Lett.* **1986**, *27*, 3123. (b) Schmehl, R. H.; Whitesell, L. G.; Whitten, D. G. *J. Am. Chem. Soc.* **1981**, *103*, 3761. (c) Mizuno, K.; Ichinose, N.; Otsuji, Y. *Chem. Lett.* **1985**, 455. (d) Fukuzumi, S.; Kuroda, S.; Tanaka, T. *J. Am. Chem. Soc.* **1985**, *107*, 3020. (e) Fukuzumi, S.; Koumitsu, S.; Hironaka, K.; Tanaka, T. *J. Am. Chem. Soc.* **1987**, *109*, 305.

(14) (a) Fukuzumi, S.; Okamoto, T.; Otera, J. *J. Am. Chem. Soc.* **1994**, *116*, 5503. (b) Fukuzumi, S.; Ohkubo, K.; Okamoto, T. *J. Am. Chem. Soc.* **2002**, *124*, 14147. (c) Fukuzumi, S.; Satoh, N.; Okamoto, T.; Yasui, K.; Suenobu, T.; Seko, Y.; Fujitsuka, M.; Ito, O. *J. Am. Chem. Soc.* **2001**, *123*, 7756.

(15) (a) Fukuzumi, S.; Ohkubo, K. *Chem. Eur. J.* **2000**, *6*, 4532. (b) Fukuzumi, S.; Mori, H.; Imahori, H.; Suenobu, T.; Araki, Y.; Ito, O.; Kadish, K. M. *J. Am. Chem. Soc.* **2001**, *123*, 12458. (c) Fukuzumi, S.; Fujii, Y.; Suenobu, T. *J. Am. Chem. Soc.* **2001**, *123*, 10191.

(16) (a) Fukuzumi, S.; Inada, O.; Satoh, N.; Suenobu, T.; Imahori, H. *J. Am. Chem. Soc.* **2002**, *124*, 9181. (b) Fukuzumi, S.; Yuasa, J.; Suenobu, T. *J. Am. Chem. Soc.* **2002**, *124*, 12566.

(17) (a) Fukuzumi, S.; Okamoto, K.; Imahori, H. *Angew. Chem., Int. Ed.* **2002**, *41*, 620. (b) Okamoto, K.; Imahori, H.; Fukuzumi, S. *J. Am. Chem. Soc.* **2003**, *125*, 7014. (c) Fukuzumi, S.; Okamoto, K.; Yoshida, Y.: Imahori, H.; Araki, Y.; Ito, O. *J. Am. Chem. Soc.* **2003**, *125*, 1007.

(18) (a) Okamoto, K.; Araki, Y.; Ito, O.; Fukuzumi, S. *J. Am. Chem. Soc.* **2004**, *126*, 56. (b) Okamoto, K.; Mori, Y.; Yamada, H.; Imahori, H.; Fukuzumi, S. *Chem. Eur. J.* **2004**, *10*, 474.

(19) (a) Sivaguru, J.; Shailaja, J.; Ramamurthy, V. In *Handbook of Zeolite Science and Technology*; Auerbach, S. M., Carrado, K. A., Dutta, P. K., Eds.; Marcel Dekker: New York, 2003; pp 591−720. (b) Lakshminarasimhan, P.; Thomas, K. J.; Johnston, L. J.; Ramamurthy, V. *Langmuir* **2000**, *16*, 9360.

(20) Kuusk V.; McIntire, W. S. *J. Biol. Chem.* **1994**, *269*, 26136.

(21) (a) Gorren A. C. F.; Duine, J. A. *Biochemistry* **1994**, *33*, 12202. (b) Gorren, A. C. F.; de Vries, S.; Duine, J. A. *Biochemistry* **1995**, *34*, 9748. (c) Gorren, A. C. F.; Moenne-Loccoz, P.; Backes, G.; de Vries, S.; Sanders-Loehr, J.; Duine, J. A. *Biochemistry* **1995**, *34*, 12926.

(22) Moenne-Loccoz, P.; Nakamura, N.; Itoh, S.; Fukuzumi, S.; Gorren, A. C. F.; Duine, J. A.; Sanders-Loehr, J. *Biochemistry* **1996**, *35*, 4713.

(23) (a) Bishop G. R.; Davidson, V. L. *Biochemistry* **1997**, *36*, 13586. (b) Zhu, Z.; Davidson, V. L. *Biochem. J.* **1998**, *329*, 175. (c) Sun, D.; Davidson, V. L. *Biochemistry* **2001**, *40*, 12285.

(24) Stowell, M. H. B.; McPhillips, T.; Rees, D. C.; Soltis, S. M.; Abresch, E.; Feher, G. *Science* **1997**, *276*, 812.

(25) (a) Rohrer, M.; MacMillan, F.; Prisner, T. F.; Gardiner, A. T.; Möbius, K.; Lubitz, W. *J. Phys. Chem. B* **1998**, *102*, 4648. (b) Donato, M. D.; Peluso, A.; Villani, G. *J. Phys. Chem. B* **2004**, *108*, 3068.

(26) (a) Graige, M. S.; Feher, G.; Okamura, M. Y. *Proc. Natl. Acad. Sci. U.S.A.* **1998**, *95*, 11679. (b) Rabenstein, B.; Ullmann, G. M.; Knapp, E.-W. *Biochemistry* **2000**, *39*, 10487. (c) Ermler, U.; Fritzsch, G.; Buchanan, S. K.; Michel, H. *Structure* **1994**, *2*, 925.

(27) Ishikita, H.; Morra, G.; Knapp, E.-W. *Biochemistry* **2003**, *42*, 3882.

(28) (a) Hutter, M. C.; Hughes, J. M.; Reimers, J. R.; Hush, N. S. *J. Phys. Chem. B* **1999**, *103*, 4906. (b) Harvey, S. C. *Proteins* **1989**, *5*, 78.

(29) For the salt effects on the radical ion pair produced in photoinduced electron transfer, see: (a) Thompson, P. A.; Simon, J. D. *J. Am. Chem. Soc.* **1993**, *115*, 5657. (b) Bockman, T. M.; Hubig, S. M.; Kochi, J. K. *J. Am. Chem. Soc.* **1998**, *120*, 2826. (c) Yabe, T.; Kochi, J. K. *J. Am. Chem. Soc.* **1992**, *114*, 4491. (d) Bockman, T. M.; Kochi, J. K. *New J. Chem.* **1992**, *16*, 39. (e) Grosso, V. N.; Previtali, C. M.; Chesta, C. A. *Photochem. Photobiol.* **1998**, *68*, 481. (f) Marcus, R. A. *J. Phys. Chem. B* **1998**, *102*, 10071. (g) Kluge, T.; Knoll, H. *Photochem. Photobiol. A* **2000**, *130*, 95. (h) Vakarin, E. V.; Holovko, M. F.; Piotrowiak, P. *Chem. Phys. Lett.* **2002**, *363*, 7.

(30) (a) Dubois, D.; Moninot, G.; Kutner, W.; Jones, M. T.; Kadish, K. M. *J. Phys. Chem.* **1992**, *96*, 7137. (b) Soucaze-Guillous, B.; Kutner, W.; Jones, M. T.; Kadish, K. M. *J. Electrochem. Soc.* **1996**, *143*, 550.

(31) (a) Savéant, J.-M. *J. Phys. Chem. B* **2001**, *105*, 8995. (b) Lehmann, M. W.; Evans, D. H. *J. Phys. Chem. B* **1998**, *102*, 9928. (c) Redepenning, J.; Castro-Narro, E.; Venkataraman, G.; Mechalke, E. *J. Electroanal. Chem.* **2001**, *498*, 192.

(32) Seely, G. R.; Gust, D.; Moore, T. A.; Moore, A. L. *J. Phys. Chem.* **1994**, *98*, 10659.

(33) (a) Marcus, R. A. *Annu. Rev. Phys. Chem.* **1964**, *15*, 155. (b) Marcus, R. A. *Angew. Chem., Int. Ed. Engl.* **1993**, *32*, 1111. (c) Marcus, R. A.; Sutin, N. *Biochim. Biophys. Acta* **1985**, *811*, 265.

(34) Perrin, D. D.; Armarego, W. L. F.; Perrin, D. R., *Purification of Laboratory Chemicals*, 4th ed.; Pergamon Press: Elmsford, NY, 1996.

(35) Bruinink, J.; Kregting, C. G. A.; Ponjee, J. J. *J. Electrochem. Soc.* **1977**, *124*, 1854.

(36) Fukuzumi, S.; Imahori, H.; Okamoto, K.; Yamada, H.; Fujitsuka, M.; Ito, O.; Guldi, D. M. *J. Phys. Chem. A* **2002**, *106*, 1903.

(37) (a) Wallenfels, K.; Gellrich, M. *Chem. Ber.* **1959**, *92*, 1406. (b) Fukuzumi, S.; Suenobu, T.; Patz, M.; Hirasaka, T.; Itoh, S.; Fujitsuka, M.; Ito, O. *J. Am. Chem. Soc.* **1998**, *120*, 8060.

(38) Nguyen, K. A.; Day, P. N.; Pachter, R. *J. Phys. Chem. A* **2000**, *104*, 4748.

(39) For the absorption spectrum of $Q^{\bullet-}$, see: Fukuzumi, S.; Yorisue, T. *J. Am. Chem. Soc.* **1991**, *113*, 7764.

(40) In the case of the photoinduced electron transfer from $^3H_2P^*$ to Q, however, the plot of k_{et} vs $[NH_4PF_6]$ gives an apparent linear line because of the fast rate being close to the diffusion.

(41) The high temperature is required to observe only the 1: 1 complex between $Q^{\bullet-}$ and NH_4PF_6.

(42) Meites, L. *Polarographic Techniques*, 2nd ed.; Wiley: New York, 1965; pp 203−301.

(43) The poor solubility of NH_4PF_6 in CH_2Cl_2 has precluded the examination of the effects of NH_4PF_6 on the redox potentials of quinones in CH_2Cl_2.

(44) The ratio of the rate constant of electron transfer at 298 K is given by $\exp(0.17 \times 23060/1.987 \times 298) = 750$.

(45) The one-electron redox potentials of Q, NQ, and HV^{2+} in the presence of various concentrations of NBu_4ClO_4 and NBu_4Br are listed in Table S1 (Supporting Information).

(46) To remove the redox potential shifts for Fc^+/Fc itself by the electrolyte completely, the ΔG_{et} values were used in the Nernst plots of ΔG_{et} vs log[electrolyte].

(47) Fukuzumi, S.; Ohkubo, K.; Suenobu, T.; Kato, K.; Fujitsuka, M.; Ito, O. *J. Am. Chem. Soc.* **2001**, *123*, 8459.

(48) Lewis, F. D.; Hougland, J. L.; Markarian, S. A. *J. Phys. Chem. A* **2000**, *104*, 3261.